

Response of low to mid-latitude ionosphere to the Geomagnetic storm of September 2017

Nadia Imtiaz¹, Waqar Younas², and Majid Khan²

¹Theoretical Physics Division, PINSTECH, Nilore, Islamabad, Pakistan

²Department of Physics, Quaid-i-Azam University, Islamabad, Pakistan

Correspondence: Nadia Imtiaz (nhussain@ualberta.ca)

Abstract. We study the impact of the geomagnetic storm of 6-9 September 2017 on the low-to-mid latitude ionosphere. The prominent feature of this solar event is the sequential occurrence of the two SYM-H minima with values of -146 nT and -115 nT on 8 September at 1 : 08 UT and 13 : 56 UT, respectively. The study is based on the analysis of data from GPS stations and the magnetic observatories located at the different longitudinal sectors corresponding to Asia, Africa, America and Pacific. The GPS data are used to derive the global, regional and vertical total electron content in the four selected regions. Magnetic observatory data are used to illustrate the variation in the magnetic field, particularly in its horizontal component. It is observed that the storm time response of the vertical total electron content over the Asia/Pacific regions is earlier than over Africa and America. Overall, the positive ionospheric storm effects over the local day side sectors are associated with the ionospheric electric fields and the traveling atmospheric disturbances. The global thermospheric composition maps by Global Ultraviolet Imager exhibits a storm time variation in the O/N_2 ratio. The positive storm effects in the O/N_2 ratio occur in the low-latitudes and equatorial regions. It can be inferred that a variety of space weather phenomena such as the coronal mass ejection, the high speed solar wind stream and the solar radio flux can cause the multiple day enhancements of the vTEC in the low-to-mid latitude ionosphere during 4-14 September 2017.

1 Introduction

It is well known fact that the geomagnetic storm is a temporary variation of the Earth's magnetic field induced by the coronal mass ejection (CME) or the high speed solar wind stream (HSSWS). The most widely used descriptors of the geomagnetic storms are: the disturbance storm time (Dst) index (which measures the ring current magnetic field), the SYM-H index (which reflects the variations in the intensity of the ring current), the Kp index, the auroral electrojet (AE) index (which measures the variations in the auroral electrojet), the Ap index and the B_z component of the Interplanetary Magnetic Field (IMF) (Rostoker (1972); Gonzalez et al. (1994); Saba et al. (1997)). On the basis of the Dst index and the B_z component of the IMF, the geomagnetic storms can be categorized as follows: weak or minor storms ($Dst \leq -30$ nT, $B_z \leq -3$ nT during 1 hour), moderate storms ($Dst \leq -50$ nT, $B_z \leq -5$ nT during 2 hours), intense storms ($Dst \leq -100$ nT, $B_z \leq -10$ nT for 3 hours) and severe storms ($Dst \leq -200$ nT) (Gonzalez et al. (1994); Tsurutani et al. (1992); Loewe and Prolss (1997)). Some scientists have used the SYM-H geomagnetic index as a re-

placement of the *Dst* index due to advantage of its 1 min time resolution compared to the 1 h time resolution of the *Dst* index (Wanliss and Showalter (2006)). The 3 h value of the *Kp* index has also been used for the classification of the geomagnetic storms as: weak or minor storms ($5- \leq Kp \leq 5$), moderate storms ($Kp \geq 6$), intense storms ($7- \leq Kp \leq 7$) and severe storms ($Kp \geq 8-$) (Gosling et al. (1991)).

5 **During geomagnetic storms, the ionosphere features vary along the latitudes and longitudes also due to different current systems flowing in the magnetosphere. Therefore, geomagnetic storms produce effects that are different in the different regions of the magnetosphere.** A number of studies have been devoted to **investigation of** the storm effects in different longitudinal and latitudinal sectors. Sharma et al. (2011) investigated the low latitude ionosphere **total electron content (TEC)** response to the geomagnetic storm of August 25, 2005. On the day of **the** storm, a doubly humped peak in the TEC is
10 **observed, these have an amplitude that is almost twice that of a quiet day value.** The first peak is attributed to **the Prompt Penetration Electric Field (PPEF)** however, the second peak is due to the plasma fountain effect. **It is also found that the effect of the PPEF is almost uniform along the longitudinal direction.** Thomas et al. (2013) studied the TEC variations in the mid-latitude Northern American sector during the storm time. It is observed that the ionosphere response to the storms is **season dependent**; i.e., the storms occurring in the summer have large negative effects while winter events have a strong initial
15 positive phase with minimum negative storm effects. Moreover, the events occurring in the fall and spring have almost the same effects. Many authors have investigated the TEC variation in the polar ionosphere (Watson et al. (2016)). In this context, Shagimuratov et al. (2012) studied the storm effects in the high latitude regions using the TEC data from International Ground Station (**IGS**) network. They found an increase in the TEC at the high latitude polar regions and this disturbance propagates to the mid-latitude and equatorial regions. They also investigated that during the southward directed B_z component of the
20 **IMF**, the enhancement in the TEC is stronger than during the northward directed storm period. **The authors** also observed a strong variation in the TEC over the sub-auroral region. Astafyeva et al. (2014) analyzed the effects of super storms having $Dst < -250$ nT on the ionospheric total electron content. They investigated that depending on the intensity of the storm, the ionospheric TEC may increase from 4 to 40 times of its quiet daily value during the main phase of the storm. The maximum change in the TEC is observed in the auroral oval region.

25

Jayachandran et al. (2011) have analyzed the GPS-TEC data of the Canadian High Arctic Ionospheric network (CHAIN) to provide **clear evidences of** systematic and propagating TEC enhancements produced by the compression of the magnetosphere as a result of high solar wind dynamic pressure. By employing the GPS triangulation technique, it is found that the TEC perturbations propagate at a speed of 3 – 6 km/s in the anti-sunward direction near the noon sector and 8 km/s in the sunward
30 direction in the pre-noon low latitude sector. It is also found that these TEC perturbations are associated with the F-region electron density enhancements and with the particle precipitation due to the sudden compression of the magnetosphere. **Momani (2012)** has investigated the climatology of the ionospheric TEC at quasi-conjugate points located at different latitudes during the low solar activity in 2007 by using the GPS data. The author has provided a clear evidence of the annual, hemispheric and **equinoctial** asymmetries in the GPS-TEC at all magnetic conjugate stations. There is a number of factors that contribute
35 to the observed GPS-TEC asymmetries. For instance, the main causes of the annual asymmetry are: the geomagnetic field

topology, the Sun-Earth distance and the lower atmosphere tidal forces. The interhemispheric asymmetry is linked to the solar declination which also leads to the seasonal variations. The **equinoctial asymmetry** which is more prominent in the March equinox compared to the September is due to the interhemispheric coupling of the ionosphere. **Many authors have analyzed the St. Patrick day storm (the largest geomagnetic storm of the Solar cycle 24) by using the GPS-TEC data analysis techniques to understand the positive and negative ionospheric-storm effects due to energy transfer between the solar wind and the magnetosphere** (Fagundes et al. (2016); Nayak et al. (2016)). In this context, Nava et al. (2016) investigated the low and mid-latitude ionospheric response to the St. Patrick day storm of 2015. The storm effects are characterized by using Global **electron content (GEC) and Regional electron content (REC)** in different longitudinal sectors such as Asia, Africa, America and Pacific. The authors observed a strong enhancement in the American sector. **It is also found that** the Asian sector shows comparatively large decrease in the vertical total electron content(vTEC). They also used the spectral analysis and **of the magnetometer data** to separate the effects of the convection electric field and of the **disturbance dynamo**. Zhang et al. (2018) analyzed this event by using the GPS data of the **Crustal Movement Observation Network of China**. It is found that during the sudden storm commencement (SSC) phase, **a rapid enhancement in the ionospheric electron density distorts the structure of the northern equatorial ionization anomaly region. It is also observed that during the main phase a significant decrease in the vTEC occurs at the high latitude as compared to the lower latitude region. Moreover, the height of the peak electron density in the F2 layer also increases during the geomagnetic storm.** Watson et al. (2016) presented a study based on data of about seventeen geomagnetic storms of the solar cycle 24 with minimum $Dst < -100$ nT which occur during the period 2009 – 2015 to identify the solar sources of these geomagnetic storms. It is found that the low geomagnetic activity is associated to the weak dawn-to-dusk solar wind electric field. The author has shown that the slow CME plays a main role in the commencement of geomagnetic storms of the solar cycle 24. Astafyeva et al. (2017) presented a study based on multiple instrument data analysis to investigate the global ionospheric/thermospheric response to the geomagnetic storm of June 22, 2015. Kashcheyev et al. (2018) have made a comprehensive analysis on the basis of two great geomagnetic storms ($Dst \leq -200$ nT) which occurred on March 17 and June 22, 2015. It is found that the absence or presence of scintillation in the African sector is associated to the local time at the beginning of the storm. Another finding is that the summer storm results into the formation of plasma bubbles which propagate up to the mid-latitudes and causing strong scintillation in the GNSS signals. On the basis of this comprehensive analysis, the authors suggested that the factors such as the local time at the commencement of the storm and the season play an important role in the modeling of the ionosphere response to the solar activity. Blagoveshchensky and Sergeeva (2019) presented a study based on **multi-instrument** analysis to reveal the variation in the ionospheric parameters during the geomagnetic storm of September 6-10, 2017. Kleimenova et al. (2018) studied the features of the daytime high latitude geomagnetic variations and geomagnetic **$pc5$ pulsations** during the two stage magnetic storm of September 7-8, 2017. They found that the daytime polar substorm prohibits the excitation of geomagnetic **$pc5$ pulsations** over the entire latitude range in which these pulsations were recorded before the daytime bay.

Present work aims to investigate the response of low-mid latitude ionosphere to the large geomagnetic storm of September 6-9, 2017. The storm effects are analyzed by using the data from the individual GNSS receivers and the magnetometer observatories located in the three different longitudinal sectors. The approach used in the present study is similar to that used by

Nava et al. (2016) and Kashcheyev et al. (2018). The remainder of this article is organized in the following manner: Section 2 **presents a** description of the data sets, GPS stations and magnetometers used in our analysis. Section 3 briefly **describes** the case study that is the solar event and its characterization on the basis of the global plasma parameters. In section 4, we present results and a general discussion of our findings. Finally, the summary/conclusion of this study are presented.

5

2 Data Sets

The following data sets have been used in this study.

1. Solar Event: **The National Oceanic and Atmospheric Administration (NOAA) Space Weather Prediction Center (SWPC) provided information about the type of solar event which causes the ionospheric perturbations. According to NOAA SWPC, a number of space weather events observed between 4-14 September 2017. The detailed description of these events is also given by Redmon et al. (2018). Here we give an overview of these solar events. Several X-class and M-class solar flares along with the CMEs occurred during this period. On September 6, the sun emitted X2.2 and X9.3 solar flares at 8 : 57 and 11 : 53 UT, respectively. On 07 September, two solar flares; i.e., M7.3 and X1.3 were emitted at 10 : 11 and 14 : 20 UT, respectively. On 08 September 2017, M8.1 solar flare was fired off at 15 : 35 UT. On September 12, X8.3 solar flare was emitted at 15 : 35 UT. The associated earthward CMEs have induced the geomagnetic storms of different intensities in the early September 2017.**
2. Solar wind parameters: The OMNI database (<https://omniweb.gsfc.nasa.gov/form/dx1.html>) has been used to get solar wind parameters. The information about the B_z component of the IMF and the solar wind speed (V_{sw}) is provided by the ACE satellite.
3. Geomagnetic indices: The world data center for Geomagnetism (Kyoto) provides information about different geomagnetic indices, **among them the AE index, the Ap index, the Kp index and SYM-H. The SYM-H is the proxy of the ring currents and the AE index estimates the energy transfer from the solar wind to the auroral ionospheric regions (Rostoker (1972); Wanliss and Showalter (2006)).**
4. Electron Content Data: **The vTEC is extracted from the International GNSS Service Global Ionosphere Map (IGS-GIM) data that are available in the standard IONEX format on the NASA's website; i.e., Crustal Dynamics Data information system (<ftp://cddis.gsfc.nasa.gov/gps/products/ionex/>). These IONEX files contain the vTEC data for the entire globe. For any time, the vTEC data can be obtained from IONEX files at the time resolution of 2-h. The tomographic kriging GIMs computed by the Technical University of Catalonia (UPC), have been used to study the GEC variations during the storm period under consideration. The GEC is the total number of electrons present in the**

ionosphere at the fixed altitude of about 450 km. The GEC is obtained from the UPC-GIM data by the summation of the ν TEC values in a cell $I_{i,j}$ multiplied by a cell's area $S_{i,j}$ over all GIM cells and it is given by Afraimovich et al. (2006),

$$GEC = \sum_{i,j} I_{i,j} \cdot S_{i,j}.$$

Here i and j represent the longitude and latitude of a certain GIM cells. The latitudinal and longitudinal extent of the elementary GIM cell is about 2.5° and 5° , respectively. The unit of GEC is $1GECU = 10^{32}$ electrons. The REC is the total number of electrons in the specified region of the ionosphere. Our analysis is based on the four different regions: Asia ($60^\circ : 150^\circ E$), Africa ($-30^\circ : 60^\circ E$), America ($-120^\circ : -30^\circ E$) and **Pacific** ($-180^\circ : -120^\circ E$; $150^\circ : 180^\circ E$). The REC is calculated **similarly to the GEC**, with the summation **being** restricted to the GIM cells of that particular region. **For both GEC/REC, the UPC-GIM data at time resolution of 15 min have been used.**

5

5. GPS stations: The data of nine GPS stations **are** analyzed here. These stations are selected on the basis of data availability and their geographic/geomagnetic location. The geographic **and geomagnetic locations** of these stations are given in Table 1.
6. Magnetometer Data: The storm time magnetic field variations are analyzed by using the data from the three low latitude observatories in three sectors: Asia (KOU), Africa (MBO) and America (GUA). The **quasi-definitive data** of these observatories which are available at <http://intermagnet.org> have been used for the analysis. Table 2 **shows geographic and geomagnetic locations** of these observatories. **In order to calculate the magnetic field variations we adopted the approach of Nava et al. (2016); Kashcheyev et al. (2018). The brief description of this approach is given here. During the geomagnetic storm, the horizontal component 'H' of the Earth's magnetic field can be expressed as:**

$$H = H_o + D_M + D_{iono} + S_R^H,$$

where H_o represents the magnetic field component due to Earth's external core dynamics, D_M is the disturbance which comes from the magnetospheric currents mainly due to Chapman Ferraro current, ring current and tail current Cole (1966). It can be calculated as:

$$D_M = \text{SYM-H} \cdot \cos\phi,$$

here ϕ is the geomagnetic latitude. The S_R^H is the quiet daily regular variation of H and is computed by using the four quietest days having $Kp < 2$ such as:

$$S_R^H = \frac{1}{n} \sum_{i=1}^n (H_i + D_i^H) - H_o,$$

where n is the number of quiet days. The D_i^H depicts the disturbances coming from the ionosphere D_{iono} and the magnetosphere D_M . The magnetic disturbance due to ionospheric electric currents can be written as:

$$D_{iono} = \Delta H - S_q - \text{SYM-H} \cdot \cos\phi,$$

here $S_q = \langle S_R^H \rangle$ is the hourly amplitude of daily variations of the geomagnetic field.

7. Thermospheric Composition: For the analysis of the storm time variation in the thermospheric neutral composition, the global maps of O/N_2 obtained from the GUVI/TIMED are presented here.

3 Case Study

- 5 In early September 2017 mainly three CMEs with the earthward trajectories were emitted on 4, 6 and 10 September. A CME originating from the massive X9.3 solar flare of 6 September, reached the Earth at 23 : 00 UT on 7 September. The arrival of this CME caused a significant compression to the dayside magnetosphere which provoked a severe geomagnetic storm having 3 h maximum value of the geomagnetic index $Kp_{max} = 8$. However, the arrival of the other two CMEs on 6 and 12 September lead to a minor geomagnetic storm of G1 category. Figure 1 illustrates the global morphology of these solar events. In Figure 1, the storm time variations of the various interplanetary plasma and field parameters are depicted in the following order (from top to bottom): the solar wind speed (V_{sw}), the B_z component of the IMF, the Interplanetary Electric Field (IEF), the AE index, the SYM-H index and the Solar radio flux $F_{10.7}$. The three vertical lines represent the CMEs which lead to the Sudden Storm Commencement (SSC) at 23 : 43, 23 : 00 and 20 : 02 UT on 6, 7 and 12 September, respectively. As reported by <http://www.obsebre.es/php/geomagnetisme/vrapides/>.
10
15 However, the present study focus on the effects of the G4 category storm which occurs on 8 September 2017. On the arrival of the interplanetary shock on 7 September at about 23 : 00 UT, the initial phase of the storm begins with a rapid variations in the above mentioned parameters. During the main phase, the B_z component of the IMF is more southward reaching the maximum lowest value of about -32 nT and then it rapidly increases to the value of approximately $+16$ nT. It again performs a negative excursion and reaches the value of approximately -16 nT. It can be seen that the
20 SYM-H index also follows the behavior of the B_z component. During the main phase of the storm, the SYM-H index also decreases and reaches the negative value of $\simeq -146$ nT thus producing the first minima of the SYM-H index at 1 : 08 UT. From 1 : 08 UT until 11 : 00 UT the B_z in northward; i.e., it increases to the positive value. Following the B_z , the SYM-H also increases from -146 nT to the value of -38 nT. During this partial recovery phase the B_z becomes southward again by performing a negative excursion of -17.6 nT at 11 : 55 UT and remains southward until 13 : 56
25 UT. At the same time the SYM-H index also reaches the second minimum value of $\simeq -115$ nT. This is the end of the main phase of the storm which lasted for ~ 15 h. The main phase can be characterized by the occurrence of the two pronounced minima of the SYM-H with values -146 nT and -115 nT at 1 : 08 UT and 13 : 56 UT respectively on 8 September 2017. The recovery phase started after 13 : 56 UT on 8 September, the SYM-H increases slowly and returned to its normal value at 14 : 00 UT on 11 September. The recovery phase lasted for about 3 days.
30 On September 8, the V_{sw} also exhibits an abrupt change by attaining a maximum value of about 820 km/s around 02 : 00 UT and after 12 : 00 UT it gradually decreases. The IEF is the E_y component of the electric field which is calculated as $E = -V_{sw} \times B$. It depends on the B_z component of the IMF and the x component of the V_{sw} . It means that the positive northward IMF leads to the westward IEF on the dayside and eastward field on the nightside. It can be seen

that the IEF fluctuation occurs between -15 and $+20$ mV/m during this storm. The next two plots represent the AE and Kp indices. The AE index shows several peaks during this period. After the arrival of CME1, there is an increase in the auroral activity such that the AE index reaches the peak value of about 1430 nT on 07 September at 09 : 07 UT. However, the occurrence of the two strong peaks exceeding 2000 nT in the AE index indicates that the most intense auroral activity occurred after the arrival of CME2. The Kp index shows the two episodes of the maximum value of approximately $K_p = +8$ for 3 h between 0 – 3 UT and 12 – 15 UT on 8 September. The bottom plot illustrates variation in the solar radio flux $F_{10.7}$. It can be seen that the solar flux fluctuates significantly during the period 4-14 September 2017.

4 Results/Discussion

In this section, we present variations of the diverse parameters such as the REC, the GEC, the vTEC, the H component of the magnetic field and the O/N_2 ratio as a result of the geomagnetic storm of 7-9 September 2017. Figure 2 shows the Δ REC (top), the Δ GEC (middle) and the SYM-H index (bottom) during the period September 4-14, 2017. **Both the Δ REC and Δ GEC are calculated by subtracting the quiet time variation from the value itself. The quiet time variation is computed using the three quiet days before the storm having the Ap index below 22 nT. The quiet days considered are 2, 3 and 4 September 2017.** It can be seen that the GEC shows two positive peaks at 1 : 08 UT and 13 : 56 UT corresponding to the first and second minima of the SYM-H index, respectively. In order to find the region which contributed to the peaks in the GEC, the REC is plotted for the four longitudinal sectors: Asia, Africa, America and Pacific. **It can be seen that during the period 4-14 September 2017, the REC varies significantly over the four longitudinal sectors. The observed behavior of the Δ REC can be attributed to the energy inputs from the solar wind to the magnetosphere Nava et al. (2016). The AE index which is an indicator of the energy transfer from the solar wind to the magnetosphere is shown in Figure 2. It can be noticed that the AE index shows several episodes of the energy inputs (having the maximum value of the AE index greater than 1000 nT) which occur on 4, 7, 8 and 13 September. In response to these energy inputs, the amplitude and the occurrence time of maxima/minima of the REC also vary.**

It is now clear that the first peak in the GEC is due to the Asian/Pacific sectors and the second peak is due to the African/American sectors. **It can be noticed that the Δ GEC plot also shows some other variation other than the the peaks. According to Afraimovich et al. (2008), there is a correlation between the GEC and the $F_{10.7}$ index. Therefore, the behavior of the GEC can also be affected by the higher solar flux; i.e., $F_{10.7} > 100$ sfu.**

The nine plots of Figure 3 illustrate the variation of the vTEC for the **individual stations** of the three longitudinal sectors from 4-14 September 2017. In Figure 3, the **plots from one to three** represent the stations of the Asian sector; i.e., BJFS, BAKO and YAR2, **the plots from four to six** represent the African sector; i.e., NOTI, NKLG and WIND. The **plots from seven to nine** represent the stations of the American sector; i.e., BOGT, AREQ and ANTC. On each plot the vTEC is **displayed** in red with **quiet daily** variations in blue which are calculated **by subtracting the quiet time variations from the value itself. The**

quiet time variations are computed by using the five quiet days before the storm having the Ap index below 22 nT. The following pertinent features of the vTEC can be noticed:

- An enhancement in the vTEC is observed for all the stations in the three longitudinal sectors on the day of the storm. The three stations in the Asian sector exhibit an increase in the vTEC at the beginning of September 8. However, the stations in the African region show the increasing trend of the vTEC in the middle and American stations on late 8 September. The variability in the occurrence of the vTEC peaks depend on the local time of the SYM-H minima at these stations.
- On the day of the storm, the northern and southern mid-latitude stations (BJFS and YAR2) in the Asian sector show an increase in the vTEC. However, in the equatorial station (BAKO) relatively less increase in the vTEC is observed.
- In the African region, the largest increase in the vTEC is observed for the equatorial and southern mid-latitude stations (NKLG and WIND) during the storm. However, a small increase in the vTEC can be seen in the northern mid-latitude station (NOTI) in this sector.
- In the American sector, the largest increase in the vTEC is observed for the equatorial station BOGT during the storm period. It can also be noticed that the vTEC decreases significantly for this station after the day of storm. Both the southern mid-latitude and equatorial trough stations ANTC and AREQ depict a multi-peak structures of the vTEC on the day of the storm. On the day after the storm the ionization disappears at the southern mid-latitudes and the vTEC returns to its quiet value.

Figure 4 illustrates the variation of vTEC as a function of time and latitudes over the four longitudinal sectors that are Asia (first plot), Africa (second plot), America (third plot) and Pacific (forth plot). **These vTEC maps are extracted from the IGS-GIM data which is available in the IONEX files for the entire globe. For a fixed longitude a contour plot covering the latitudinal range of -90° to 90° is made by using the MATLAB script. The longitudes considered are given as: $110^\circ E$ for Asia, $-10^\circ E$ for Africa, $-70^\circ E$ for America and $150^\circ E$ for Pacific.** The four vTEC maps shown in Figure 4 cover the period from 4-14 September 2017 and the latitudinal range (-90° to $+90^\circ$). The SYM-H index over this period is also shown at the bottom in Figure 4. **The space weather conditions during this period are highly disturbed due to multiple events such as the CMEs and HSSWS. As a result the vTEC maps of the four longitudinal sectors show following features:**

- **During geomagnetically quiet conditions, the $E \times B$ drift at the dip equator creates the Equatorial Ionization Anomaly (EIA) at $\pm 10 - 15^\circ$ from the equator (Balan and Bailey (1995); Fejer (1991)). In response to the geomagnetic storm the latitudinal extent of the EIA is increased upto about 30° latitudes.**
- **All the four sectors show an enhancement in the vTEC on 6 September. This behavior can be associated with the impact of the CME1 which arrived at 23:43 UT on 6 September.**
- **During the initial phase of the storm on 7 September, the vTEC enhancement mainly occurred in the crest regions of the EIA with a clear latitudinal separation.**

- On the day of the storm, the $vTEC$ strongly enhanced in the crests of the EIA and in the magnetically equatorial region as compared to the days before and after the storm. The enhancements of the $vTEC$ in the EIA region in response to the geomagnetic storms have been reported in many studies (Zhao et al. (2005); Astafyeva et al. (2015); Lei et al. (2018)).
- 5 – It can be clearly seen that the local dayside sectors such as Asia ($LT = UT + 7$) and Pacific ($LT = UT + 10$) exhibit the largest increase in the $vTEC$ on early 8 September corresponding to the first SYM-H minima. However, at the time of second minima the other two sectors that is America ($LT = UT - 5$) and Africa ($LT = UT - 1$) are on the dayside and show the largest increase in the $vTEC$.
- 10 – In the Asian sector, a regular pattern of the $vTEC$ which consists of a well defined crests can be observed except on the day of the storm. However, both the African and Pacific sectors show irregular patterns; i.e., sometimes one and sometimes two crests of the $vTEC$ appear. During the recovery phase on 9 September, the $vTEC$ return back to its normal pattern. In the American sector, we mostly observed one crest of the $vTEC$ and a very strong ionization on the day of the storm which return to its normal level after the storm on 9 September.
- 15 – An enhancement in the $vTEC$ particularly, in the crests regions of the EIA are also observed on 5 and 11 September which can be due to the HSSWS effect Nava et al. (2016).

The observed dayside positive storm phases can be explained on the basis of the two phenomena; i.e., the PPEF and the traveling atmospheric disturbances (TADs). These TADs which originated from the polar regions due to a large amount of energy deposition from the magnetosphere during the storm period (Fuller-Rowell et al. (1994)). The propagation of these TADs to low latitudes and across the equator can cause disturbance in the ionosphere by moving the plasma up and down along the magnetic field lines. According to Lei et al. (2018), the upward vertical $E \times B$ drifts are very strong between 01 – 14 UT on 8 September. These enhanced $E \times B$ drifts can be associated with the PPEF and the disturbance dynamo electric fields (DDEFs) driven by thermospheric winds (Spiro et al. (1988); Blanc and Richmond (1980)). During the main phase of the storm, the upward drifts can shift the plasma to higher altitudes where the chemical losses are very small and it can induce a super fountain effect. On the other hand, the equatorward winds can inhibit the downward diffusion of plasma (Balan et al. (2010)). The combined effect of the electric fields and thermospheric winds can lead to the enhancement of the $vTEC$ in the EIA. Besides these factors, the solar radio flux $F_{10.7}$ which varies greatly during this period as shown in Figure 2 (bottom plot) can also affect the $vTEC$ (Lei et al. (2018)).

The three plots in Figure 5 represent the **magnetic field variations** at the three equatorial magnetic observatories corresponding to the three longitudinal sectors of Asia (GUA), Africa (MBO) and America (KOU). Each plot shows the variation in the H component of the magnetic field (in black), the **quiet daily** variation (S_q) (in blue) and the ionospheric disturbances (D_{iono}) (in red). **The three dashed lines correspond to the impact of the CMEs on 6, 7 and 12 September. The following features of the H component can be noticed in all the three sectors:**

Table 1. Geographic latitude, Geographic longitude, Geomagnetic latitude and Geomagnetic longitude of the GPS stations located in different regions used in the analysis.

Station	Sector	GLAT	GLONG	MLAT	MLONG
BJFS	Asia	39.60° <i>N</i>	115.89° <i>E</i>	30.23° <i>N</i>	172.23° <i>W</i>
BAKO	Asia	6.49° <i>S</i>	106.85° <i>E</i>	16.03° <i>S</i>	179.68° <i>E</i>
YAR2	Asia	29.04° <i>S</i>	115.35° <i>E</i>	38.35° <i>S</i>	170.85° <i>W</i>
NOTI	Africa	36.87° <i>N</i>	14.98° <i>E</i>	36.43° <i>N</i>	94.94° <i>E</i>
NKLG	Africa	0.35° <i>N</i>	09.67° <i>E</i>	1.59° <i>N</i>	82.67° <i>E</i>
WIND	Africa	22.57° <i>S</i>	17.09° <i>E</i>	22.09° <i>S</i>	86.00° <i>E</i>
AREQ	America	16.50° <i>S</i>	71.50° <i>W</i>	6.82° <i>S</i>	1.30° <i>E</i>
BOGT	America	4.64° <i>N</i>	74.08° <i>W</i>	14.19° <i>N</i>	1.27° <i>W</i>
ANTC	America	37.34° <i>S</i>	71.53° <i>W</i>	27.58° <i>S</i>	1.18° <i>E</i>

Table 2. Locations of the Magnetometers used in the analysis.

Station	Sector	GLAT	GLONG	MLAT	MLONG
GUA	Asia	13.59° <i>N</i>	144.87° <i>E</i>	5.87° <i>N</i>	143.28° <i>W</i>
MBO	Africa	13.34° <i>N</i>	16.97° <i>W</i>	18.48° <i>N</i>	58.16° <i>E</i>
KOU	America	5.21° <i>N</i>	52.93° <i>W</i>	14.17° <i>N</i>	20.48° <i>E</i>

- Firstly, an increase in the H component occurred during the initial phase of the storms. This enhancement is due to the Chapman-Ferraro current resulting from the contraction of the magnetosphere (Chapman and Ferraro (1931)).
- Secondly, a strong decrease in the H component can be observed during the main phase of the storms. It can be attributed to the diamagnetic behavior of the equatorial ring current. The enhanced ring current in the magnetosphere induced the magnetic field opposite to the Earth’s northward dipole field which strongly reduces the H component (Gonzalez et al. (1994)).
- Following the strongest decrease in the H component, the recovery phase started which lasted for several hours. During the recovery phase, the ring current decays and the H component of the magnetic field returns back to the normal levels.
- Two pronounced dips in the H component at 1 : 08 UT and 13 : 56 UT on September 8 are observed in the three stations. It can be seen that the first minima is strongly negative for MBO as compared to GUA and KOU. However, the second dip is strongly negative for MBO as compared to GUA and KOU. This behavior is due to the local time variation of the ring current during the storm.

– Overall, the largest disturbance of the H component of the magnetic field with amplitude -180 nT is observed at MBO as compared to -150 nT at KOU and -140 nT at GUA.

The disturbance due to ionosphere electric current D_{iono} is represented by the red curve in Figure 5. It follows anti- S_q signature during the storm period. It can be noted that during the first southward excursion of the magnetic field, the D_{iono} , decreases at the GUA which is in the noon sector. However, an increasing trend in the D_{iono} is observed for the MBO and KOU which are in the night sector. During the second southward excursion of the magnetic field, D_{iono} decreases significantly for the MBO and KOU which are now in the dayside. The D_{iono} contains signatures of the PPEF and DDEF therefore, the observed trend of the D_{iono} can also be explained by these two electric fields. (?) Another effect that can be seen during the storm is the variation in the the thermospheric neutral composition. The storm strengthens the vertical and meridional winds which leads to the variation in the thermospheric neutral profile. The global view of the thermospheric O/N_2 ratio obtained from the TIMED/GUVI for the period September 7-10, 2017 is shown in Figure 6. On the day of the storm, a significant enhancement in the O/N_2 ratio is observed at the low and equatorial latitudes. At the same time, the O/N_2 decreases significantly at mid to high latitudes as compared to the quiet time pattern. This observation is consistent with the behavior of the $vTEC$ during the storm period. After the recovery of the storm, the thermospheric composition returns to its normal profile.

5 Conclusions

We presented the impact of geomagnetic storm of 7-9 September 2017 on the low-to-mid latitude ionosphere over the four longitudinal sectors; i.e., Asia, Africa, America and Pacific. The storm effects are characterized by using diverse parameters including the global, regional and vertical total electron content derived from the GPS data, the horizontal component of the magnetic field obtained from the magnetometers and the neutral composition from the GUVI/TIMED. It is observed that the positive storm effects occur in the local dayside stations. The temporal response of the four sectors shows that the positive storm effects in the REC and $vTEC$ over the Asian/Pacific sectors are observed earlier than the American/African sectors. During geomagnetically quiet conditions, most of the TEC is confined to the equatorial and low latitude regions. However, the latitudinal extent of the TEC increases upto the mid-latitudes during the storm period. The storm time enhancement in the neutrals ratio; i.e., O/N_2 over the low latitudes and equator is consistent with the observed TEC behavior. Overall, the positive storm phase occur on the dayside sectors during the G4 geomagnetic storm of September 7-9, 2017. The $vTEC$ enhancements observed on the other days are due to the high speed solar wind stream event. Analysis of the magnetometers data shows the largest disturbance of the horizontal component of the magnetic field at MBO as compared to that of KOU and GUA. The storm time variation of the horizontal component is associated with the Chapman-Ferraro and the ring currents. The magnetic field component associated with the disturbed ionospheric current follows the anti- S_q variations which depends on the prompt penetration electric field and the disturbance dynamo electric field. However, the negative storm effect in the O/N_2 ratio can be observed in the higher and mid-latitude regions. It can be concluded that the ionosphere dynamics and electrodynamics

play important role in the observed perturbations in the low-to-mid latitude ionosphere during 4-14 September 2017. The study would be useful for the understanding of storm time response of the low-mid latitude ionosphere.

Acknowledgements. The authors are grateful to the space weather data resources: the OMNI data base <https://omniweb.gsfc.nasa.gov/form/dx1.html> for providing the solar wind data, to the World Data Center for Geomagnetism at Kyoto University, Japan for providing the geomagnetic data: <http://wdc.kugi.kyoto-u.ac.jp/dstrealtime/>, to the International GNSS Service (IGS) team for providing the GPS data and to the <https://ssusi.jhuapl.edu/>. NI acknowledge the UNOOSA/ICTP for providing the financial support to attend GNSS workshop and learn these data analysis techniques. The authors are very grateful to the anonymous referees for their constructive and insightful comments in improving the manuscript. The authors would like to thanks Anton Kashcheyev and Christine Amory Mazaudier for their valuable suggestions. This research work was partly supported by the HEC Pakistan: *GrantNo.7632/Federal/NRPU/RD/HEC/2017*.

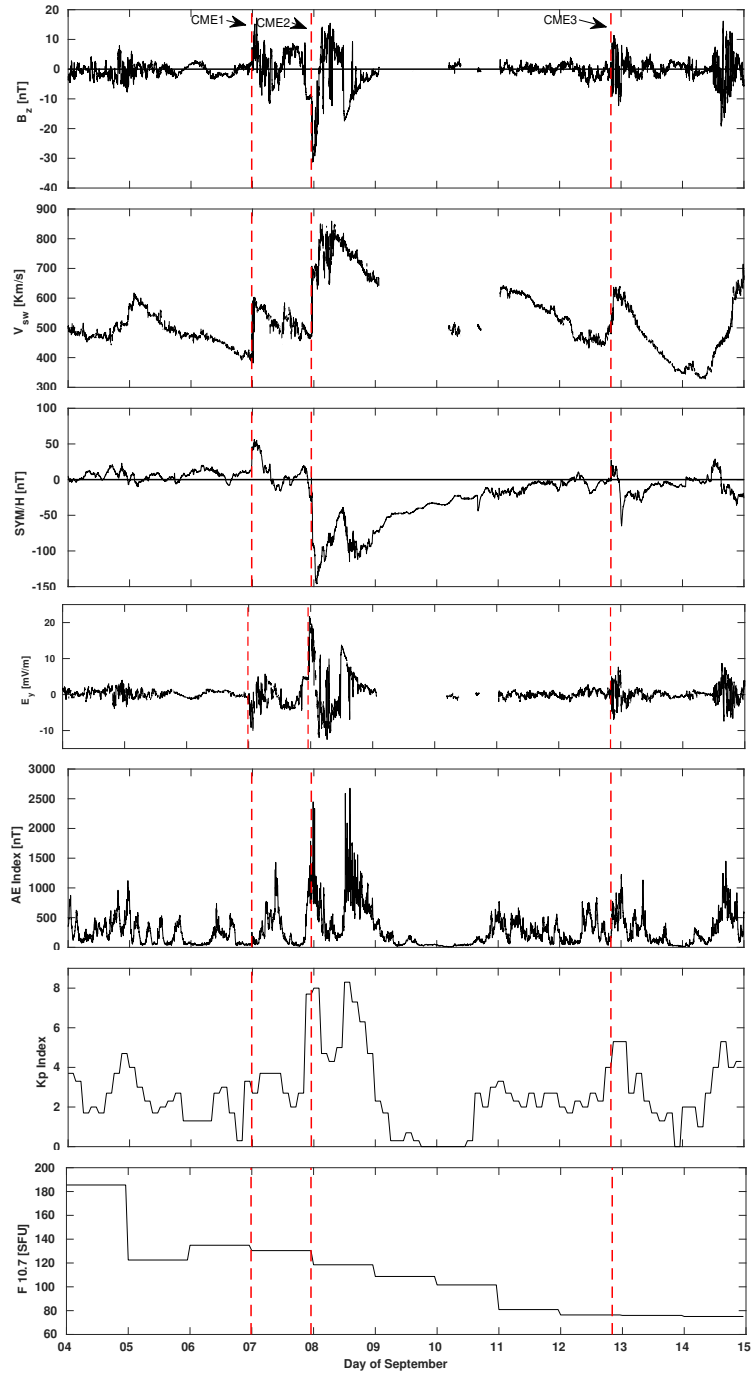


Figure 1. Global parameters: the B_z component of the IMF, the V_{sw} , the AE index, the interplanetary electric field (IEF), the SYM-H index, the Kp index and $F_{10.7}$ characterizing the geomagnetic storm during September 4-12, 2017

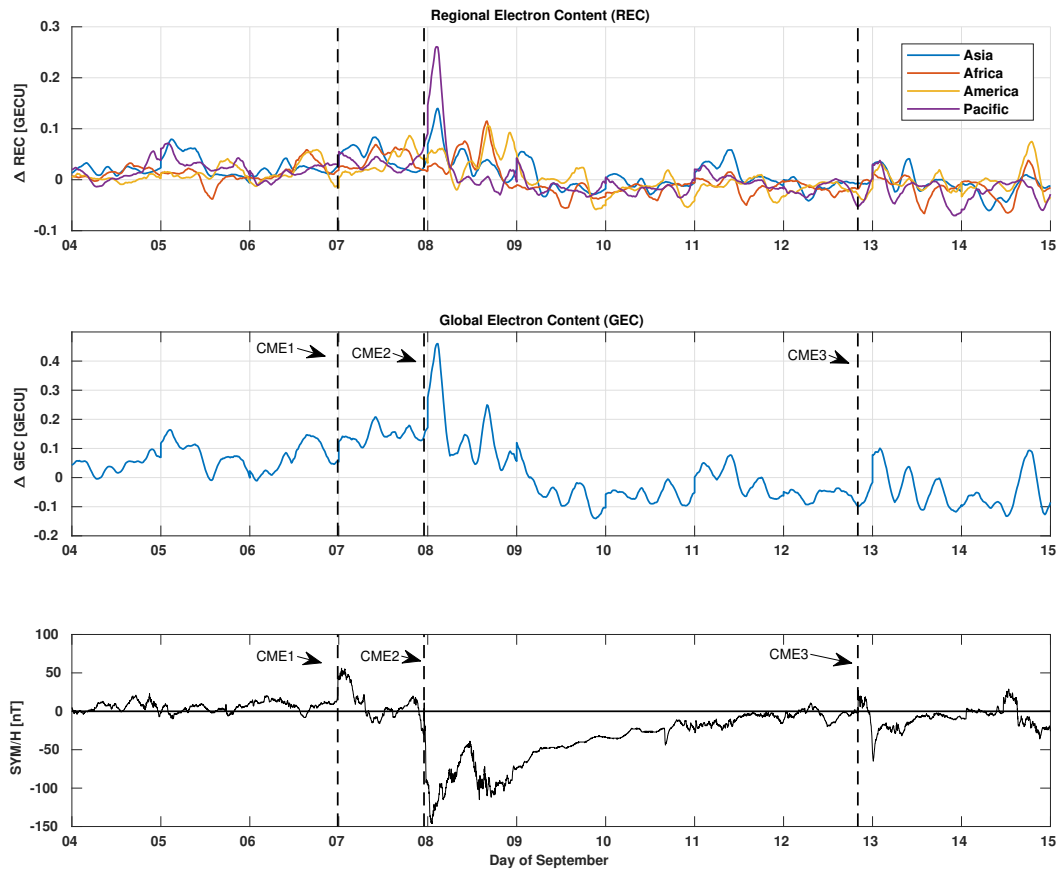


Figure 2. Variation of the Regional electron content (top), the Global electron content (bottom) and the SYM-H index during the geomagnetic storm of 4-14 September 2017

References

- Astafyeva, E., Yasyukevich, Y., Maksikov, A., and Zhivetiev, I.: Geomagnetic storms, super-storms, and their impacts on GPS-based navigation systems, *Space Weather*, 12, 508-525, **2014**.
- Astafyeva, E., Zakharenkova, I., and Förster, M.: Ionospheric response to the 2015 St. Patrick's Day storm: A global multi-instrumental overview, *J. Geophys. Res.-Space*, 120, 9023–9037, **2015**.
- Astafyeva, E., Zakharenkova, I., Huba, J. D., Doonbas, E., and Van den IJssel, J.: Global Ionospheric and Thermospheric Effects of the June 2015 Geomagnetic Disturbances: Multi-Instrumental Observations and Modeling, *J. Geophys.*, 122, 716-742, **2017**.
- Afraimovich, E. L., Astafyeva, E., and Zhivetiev, I. V.: Solar activity and Global electron content, *Dokl. Earth Sci.*, 409(2), 921-924, **2006**.
- Afraimovich, E. L., Astafyeva, E. I., Oinats, A. V., Yasukevich, Y. V., and Zhivetiev I. V.: Global electron content: A new conception to track solar activity, *Ann. Geophys.*, 26, 335–344, **2008**.

- Balan, N., and Bailey, G.J.: Equatorial plasma fountain and its effect; Possibility of an additional layer, *J. Geophys. Res.*, 100, 21421-21432, **1995**.
- Balan, N., Shiokawa, K., Otsuka, Y., Kikuchi, T., Lekshmi, D. V., Kawamura, S., Yamamoto, M., and Bailey, G. J.: A physical mechanism of positive ionospheric storms at low and mid latitudes through observations and modeling, *J. Geophys. Res.*, 115, A02304, doi:10.1029/2009JA014515, **2010**.
- 5 Blagoveshchensky, D. V., and Sergeeva, M. A.: Impact of geomagnetic storm of September 7–8, 2017 on ionosphere and HF propagation: A **multi-instrument** study, *Advan. in Space Res.*, 63, 239-256, **2019**.
- Blanc, M. and Richmond, A. D.: The ionospheric disturbance dynamo, *J. Geophys. Res.*, 85, 1669–1686, **1980**.
- Fejer, B.G.: Low latitude electrodynamic plasma drifts, *J. Atm. Terr. Phys.*, 53, N8, 677-693, **1991**.
- 10 Fuller-Rowell, T. J., Codrescu, M. V., Moffett, R. J., and Quegan, S.: Response of the thermosphere and ionosphere to geomagnetic storms, *J. Geophys. Res.*, 99(A3), 3893–3914, doi:10.1029/93JA02015, **1994**
- Cole, K. D.: Magnetic Storms and Associated Phenomena, *Space Science Reviews*, 5, 699–770, doi: 10.1007/BF00173103, **1966**.
- Chapman, S., and Ferraro, V. C. A.: New theory of magnetic storms, *Terr. Magn. Atmos. Electr.*, 36, 77–97, **1931**.
- Fagundes, P. R., Cardoso, F. A., Fejer, B. G., Venkatesh, K., Ribeiro, A. G. B., and Pillat, V. G.: Positive and negative GPS-TEC ionospheric storm effects during the extreme space weather event of March 2015 over the Brazilian sector, *J. Geophys. Res.*, 121, 5613-5625, **2016**.
- 15 Rostoker, G.: Geomagnetic indices, *J. Geophys. Res.*, 10, 935-950, <https://doi.org/10.1029/RG010i004p00935>, **1972**.
- Gonzalez, W.D., Joselyn, J. A., Kamide, Y., Kroehl, H. W., Rostoker, G., Tsurutani, B. T., and Vasyliunas, V. M.: What is a geomagnetic storm?, *J. Geophys. Res.*, 99 (A4), 5771-5792, **1994**.
- Gosling, J. T., McComas, D. J., Phillips, J. L., and Bame, S. J.: Geomagnetic activity associated with earth passage of interplanetary shock disturbances and coronal mass ejections, *J. Geophys. Res. Space*, 96, 7831–7839, **1991**.
- 20 Jayachandran, P. T., Watson, C., Rae, I. J., MacDougall, J. W., Chadwick, R., Kelly, T. D., Prikryl, P., Meziane, K., Danskin, D. W., and Shiokawa, K.: High-latitude GPS TEC changes associated with a sudden magnetospheric compression, *J. Geophys. Res.*, 38, **2011**.
- Kashcheyev, A., Migoya-Oru , Y., Amory-Mazaudier, C., Fleury, R., Nava, B., Alazo-Cuartas, K., and Radicella, S.M.: Multi-variable comprehensive analysis of two great geomagnetic storms of 2015, *J. Geophys. Res.*, 123, 5000-5018, **2018**.
- 25 Kleimenova, N. G., Gromova, L. I., and Malysheva, L. M.: Large Magnetic Storm on September 7-8, 2017: High-Latitude Geomagnetic Variations and Geomagnetic Pc5 Pulsations, *Geomagnetism and Aeronomy*, 58, 597-606, **2018**.
- Lei, J., Huang, F., Chen, X., Zhong, J., Ren, D., Wang, W., et al.: Was magnetic storm the only driver of the long-duration enhancements of daytime total electron content in the Asian-Australian sector between 7 and 12 September 2017?, *J. Geophys. Res.*, 123, 3217–3232. <https://doi.org/10.1029/2017JA025166>, **2018**.
- 30 Loewe, C. A., and Prolls, G. W.: Classification and mean behavior of magnetic storms, *J. Geophys. Res.*, 102, 209–213, **1997**.
- Momani, M. A.: GPS observations at quasi-conjugate points under solar Minimum, *Radio Science*, 47, 1-12, **2012**.
- Mannucci, A.J., Tsurutani, B.T., Iijima, B.A., Komjathy, A., Saito, A., Gonzalez, W.D., Guarnieri, F.L., Kozyra, J.U., and Skoug, R.: Dayside global ionospheric response to the major interplanetary events of October 29-30, 2003 “Halloween Storms”, *Geophys. Res. Lett.*, 32, 12, DOI 10.29/2004GL021467, **2005**.
- 35 Nayak, C., Tsai, L.-C. Su, S.-Y., Galkin, I. A., Tan, A.T.K., Nofri, E., and Jamjareegulgarn, P.: Peculiar features of the low-latitude and midlatitude ionospheric response to the St. Patrick’s Day geomagnetic storm of 17 March 2015, *J. Geophys. Res.*, 121, 7941-7960, **2016**.
- Nava, B., Zuluaga, J. R., Alazo-Cuartas, K., Kashcheyev, A., Migoya-Oru , Y., Radicella, S. M., Mazaudier, C. A., and Fleury, R.: Middle and low latitude ionosphere response to 2015 St. Patrick’s Day geomagnetic storm, *J. Geophys. Res.*, 121, 3421-3438, **2016**.

- Redmon, R. J., Seaton, D. B., Steenburgh, R., He, J., and Rodriguez, J. V.: September 2017s geoeffective space weather and impacts to Caribbean radio communications during hurricane response, *Space Weather*, 16, 1190–1201, **2018**.
- Fares Saba, M. M., Gonzalez, W. D., and CluÂa de Gonzalez, A. L.: Relationships between the AE, ap and Dst indices near solar minimum (1974) and at solar maximum (1979), *Ann. Geophysicae* 15, 1265-1270, (**1997**).
- 5 Shagimuratov, I. I., Krankowski, A., Ephishov, I., Cherniak, Y., Wielgosz, P., and Zakharenkova, I.: High latitude TEC fluctuations and irregularity oval during geomagnetic storms, *Advances in Space Res.*, 64, 521-529, **2012**.
- Sharma, S., Galav, P., Dashora, N., Alex, S., Dabas, R.S., and Pandey, R.: Response of low-latitude ionospheric total electron content to the geomagnetic storm of 24 August 2005, *J. Geophys. Res.*, 116, 1-12, **2011**.
- Spiro, R. W., Wolf, R. A., and Fejer, B. G.: Penetration of high latitude-electric-field effects to low latitudes during SUNDIAL 1984, *Ann. Geophys.*, 6, 39–50, **1988**.
- 10 Thomas, E.G., Baker, J. B. H., Ruohoniemi, J. M., Coster, A. J., Foster, C., and Erickson, P. J.: Direct observations of the role of convection electric field in the formation of a polar tongue of ionization from storm enhanced density, *J. Geophys. Res.*, 118, 1180-1189, **2013**.
- Tsurutani, B. T., Lee, Y. T., Gonzalez, W. D., and Tang, F.: Great Magnetic Storms, *Geophys. Res. Letter*, 19, 73–76, doi: 10.1029/91GL02783, **1992**.
- 15 Tsurutani, B., Mannucci A., Iijima, B., Abdu, M.A., Sobral, J.H.A., Gonzalez, W., Guarneri, F., Tsuda, T. et al.: Global dayside ionospheric uplift and enhancement associated with interplanetary electric fields, *J. Geophys. Res.* 109, A08302, **2004**.
- Tsurutani, B.T., Verkhoglyadova, O.P., Mannucci, A.J., Saito, A., Araki, T., Yumoto, K., Tsuda, T., Abdu, M.A., Sobral, J.H.A., Gonzalez, W.D., McCreddie, H., Lakhina, G.S. and Vasyliunas, V.M.: Prompt penetration electric fields (PPEFs) and their ionospheric effects during the great magnetic storm of 30–31 October 2003 , *J. Geophys. Res.*, 113, A05311, doi:10.1029/2007JA012879, **2008**.
- 20 Watson, C., Jayachandran, P. T., and MacDougall, J. W.: Characteristics of GPS TEC variations in the polar cap ionosphere, *J. Geophys. Res.*, 121, 1-22, **2016**.
- Wanliss J. A. and Showalter K. M.: High-resolution global storm index: Dst versus SYM-H, *J. Geophys. Res.*, 111, A02202, doi:10.1029/2005JA011034, **2006**.
- Zhang, W., Zhao, X., Jin, S. and Li, J.: Ionospheric disturbances following the March 2015 geomagnetic storm from GPS observations in
25 China, *Geodesy and Geodynamics*, 9, 288-295, **2018**.
- Zhao, B., Wan, W., and Liu, L.: Responses of equatorial anomaly to the October–November 2003 superstorms, *Ann. Geophys.*, 23, 693–706, <https://doi.org/10.5194/angeo-23-693-2005>, **2005**.

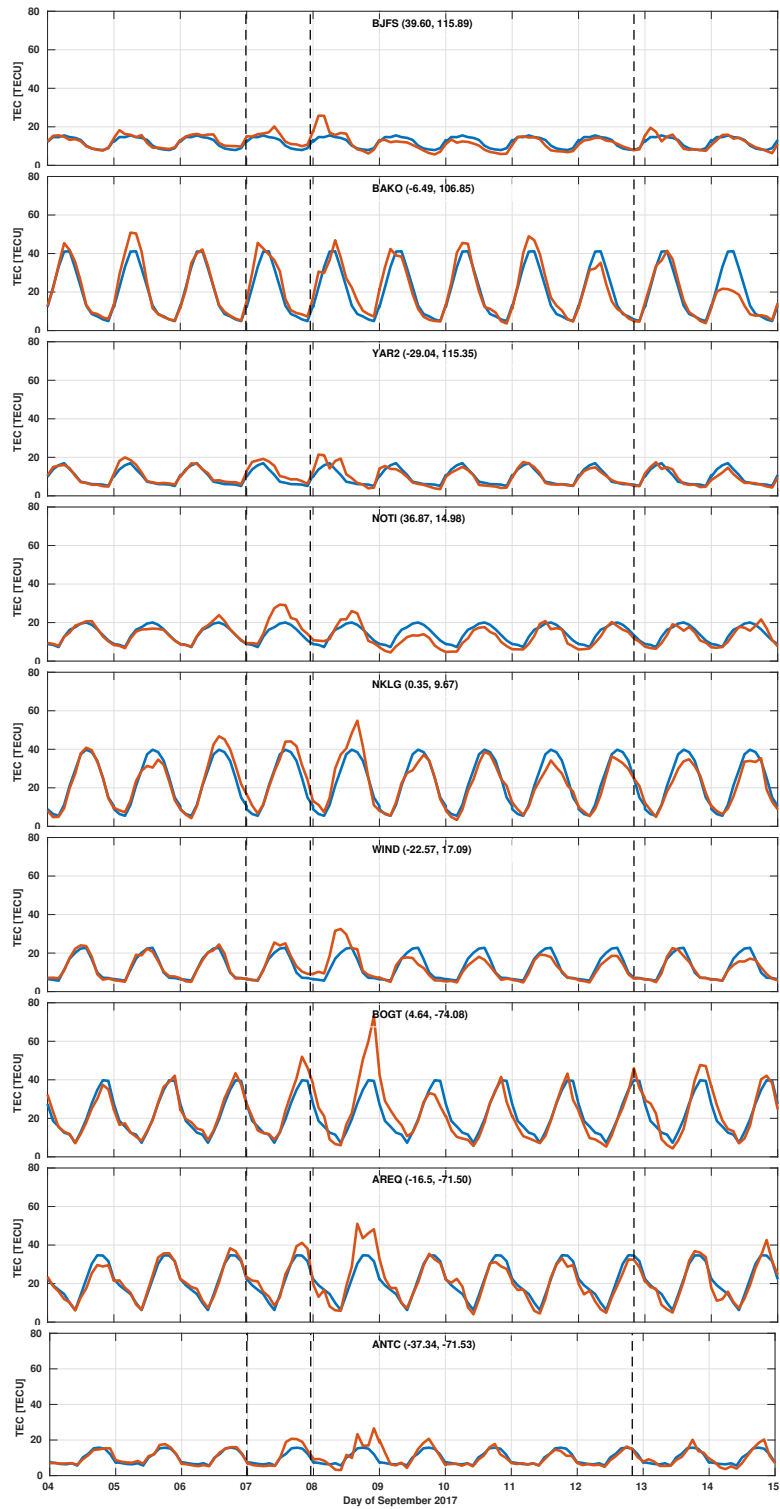


Figure 3. The $vTEC$ variations at GPS stations during the geomagnetic storm of 4-14 September 2017. Each plot illustrates the disturbed $vTEC$ (in orange) and its quiet value (in blue).

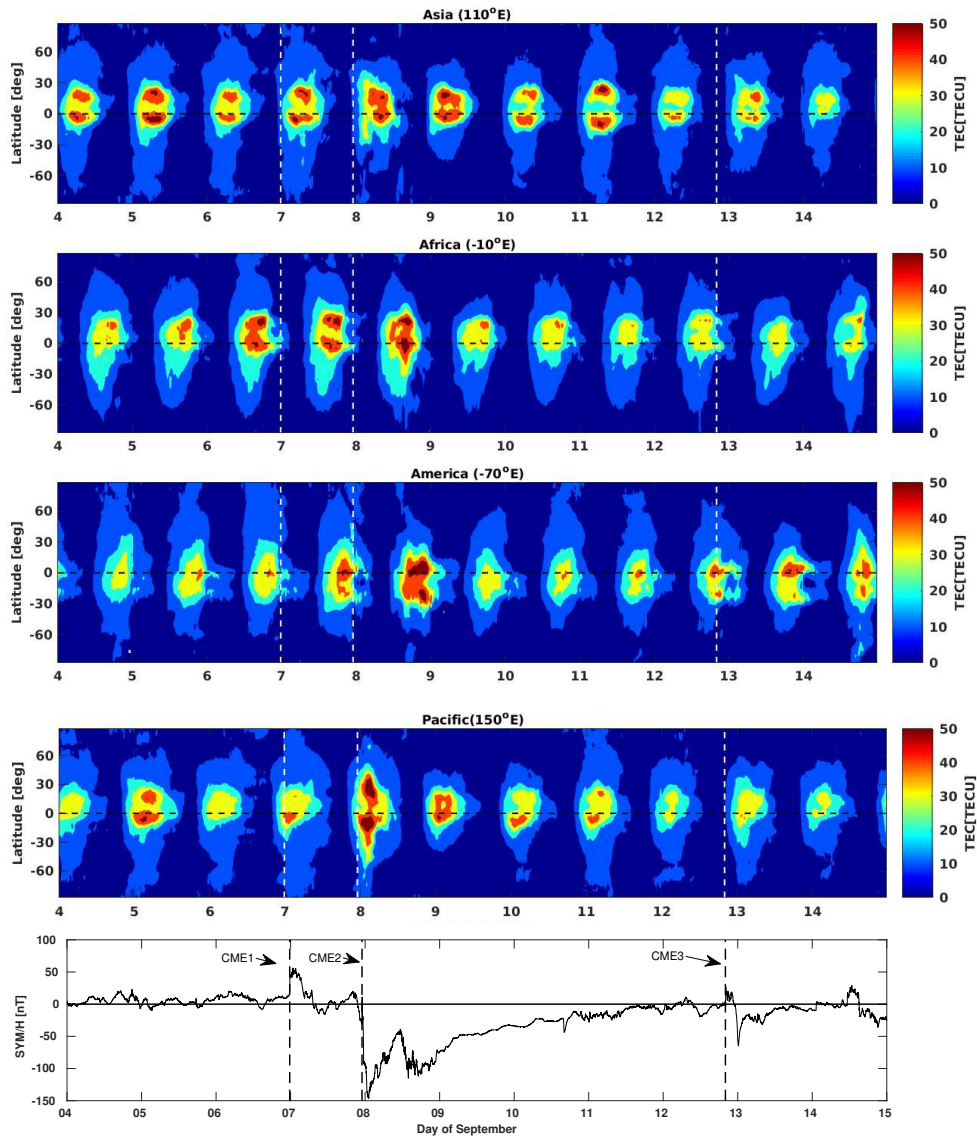


Figure 4. The vTEC variations over the Asian (first plot), African (second plot), American (third plot), Pacific (fourth plot) sectors and the SYM-H index (bottom plot) during the geomagnetic storm of 4-14 September 2017

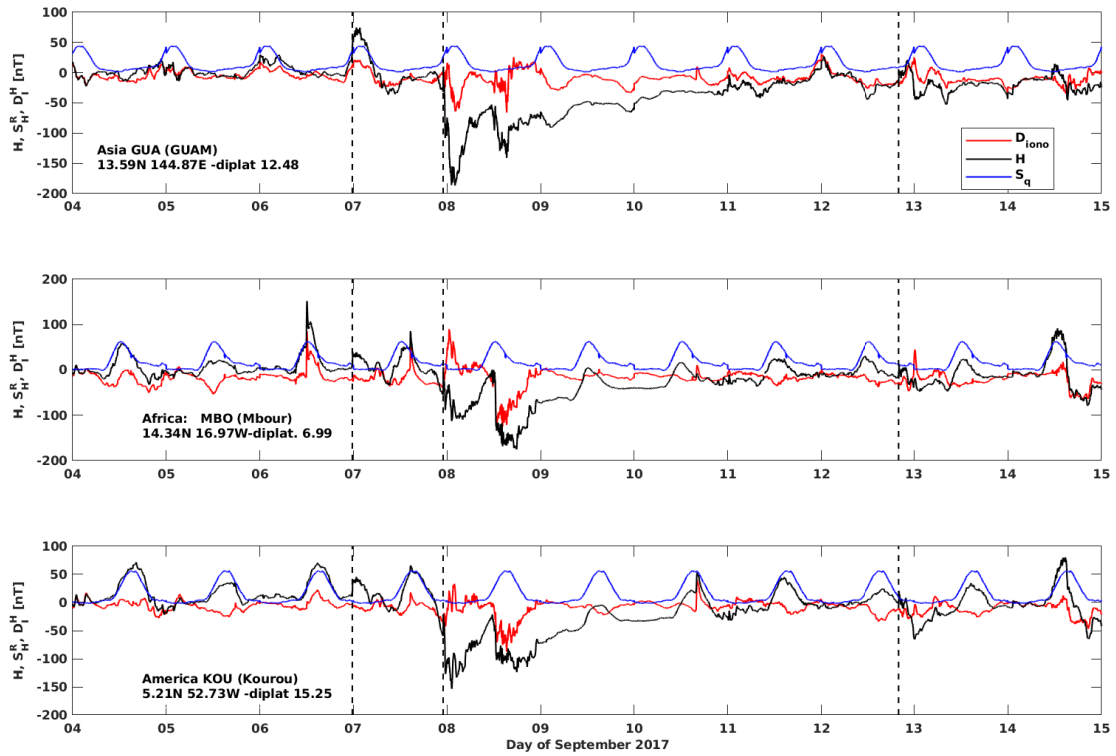


Figure 5. The magnetometer H variations at specific stations during 4-14 September 2017 over the three sectors: the Asian (top), the African (middle) and the American (bottom). On each plot the **quiet daily** variations (blue), the actual H variations (black) and the ionosphere disturbance current (**red**) are plotted

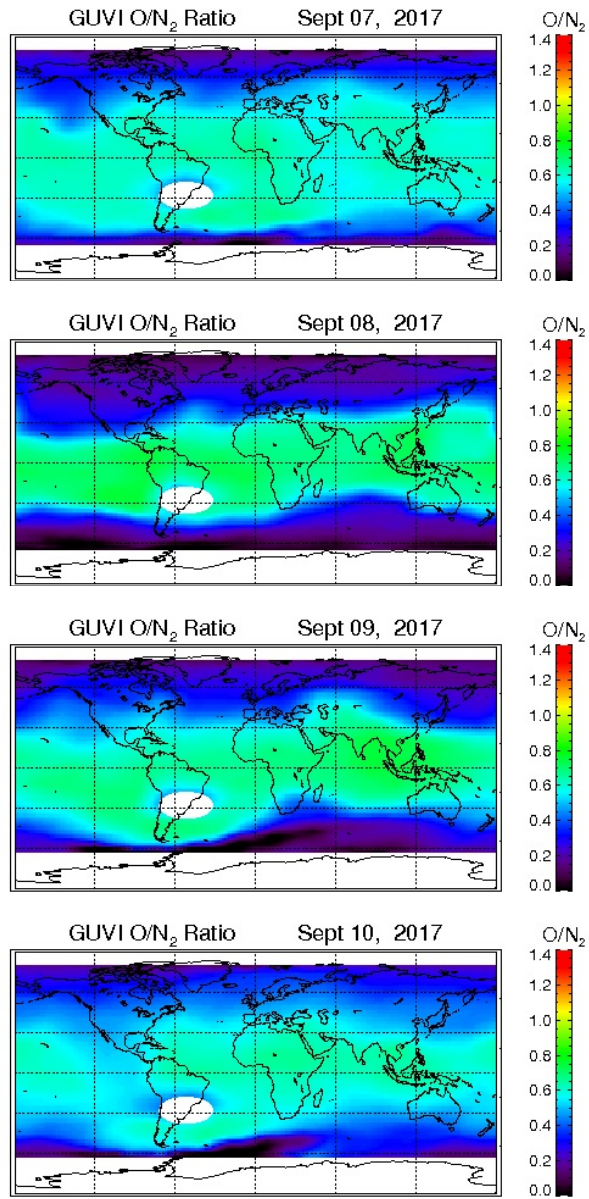


Figure 6. The thermospheric O/N_2 ratio obtained from the GUVI/TIMED during G4 category storm which occurred between 7-10 September 2017